forum acusticum 2026
8-12 September · Graz, Austria

LONG-RANGE OUTDOOR ACOUSTIC SIMULATION WITH 3D FDTD USING THE QUASI-WAVELET APPROACH OF TURBULENCE

Sophia Julia Feriani[1], Hazael Montanaro[1], Reto Pieren[1]

[1] *Acoustics/Noise Control, Empa, Überlandstrasse 129, 8600 Dübendorf, Switzerland*

Abstract

In outdoor acoustics, sound propagation is impacted by meteorological conditions, including atmospheric turbulence, which can cause significant fluctuations in sound pressure. To numerically model the propagation of sound in an inhomogeneous atmosphere, the quasi-wavelet approach is a useful representation of the random turbulent field created by temperature and velocity-induced turbulence. In this paper, the quasi-wavelet approach is implemented in a GPU-accelerated solver of the 3D acoustic wave equation, using the Finite-Difference Time-Domain method; this solver includes a moving window feature to enable computationally efficient long-range simulations. We predict the sound propagation from a point source to a distant receiver, both located near a flat terrain and surrounded by an adequate PML formulation. The temperature and the velocity-induced turbulence are first introduced separately and then their effect is combined. For a set of representative cases of meteorological conditions, the coherence loss in ground effect is calculated between the non-turbulent and the turbulent case to assess the scale of each type of turbulence.

Keywords: *Outdoor sound propagation, Finite Difference Time Domain, meteorological effects, quasi-wavelet*

1. Introduction

The outdoor sound propagation of an acoustic wave in air can be modeled numerically using the Finite Difference Time Domain (FDTD) method [1]. Meteorological phenomena such as wind, temperature and density variations, cause atmospheric turbulence and affect the sound propagation in outdoor settings. Therefore, to generate valid numerical results, the atmosphere must be accurately characterized by including the relevant meteorological effects in the numerical model. The FDTD method is a numerical method capable of handling complex propagation phenomena [2], [3], including atmospheric turbulence [4].

To model atmospheric turbulence, the quasi-wavelet approach is a practical way of introducing controlled scattering of the acoustic wave in the computational domain of the FDTD method. A quasi-wavelet (QW) is a self-similar localized function, analogous to classic wavelets [5] but their orientation and position are random. A collection of QWs behave like eddies so they can be designed to model the acoustic scattering due to turbulence [6]. First, the QW model was shown to have a similar behavior as the von Kármán spectrum for velocity-induced turbulence [7]. Then, it was also shown to accurately represent simple turbulence situation for temperature-induced turbulence [8] and later extended to induce more complex random fields [9].

In this paper, the QW approach is used to numerically model four representative turbulent atmospheres. In a large 3D computational domain, the sound wave propagates in the atmosphere over a distance of 100 m. The speed of sound of each grid point is evaluated by the QW approach to account for the variations from temperature or velocity-induced turbulence, via the effective speed of sound. Since the sound propagation is near the ground, the elevation angle of the propagation from the sound to the receiver is small. The effective sound speed approximation is therefore valid [10]. Our findings provide new insights in the numerical modeling of atmospheric turbulence by comparing the numerical results to the theoretical coherence loss in the corresponding turbulent atmosphere.

2. Method

2.1. Acoustics wave equation

The governing equations of the acoustic wave propagation in a homogeneous atmosphere are as follows:

Corresponding author: *sophia.feriani@empa.ch.*

$$
\begin{aligned}
\frac{\partial p}{\partial t} &= -\rho c^2 \nabla \cdot \mathbf{v} \\
\frac{\partial \mathbf{v}}{\partial t} &= -\frac{1}{\rho} \nabla p
\end{aligned}
\tag{1}
$$

where p is the sound pressure in Pa, $\mathbf{v}$ is the 3D particle velocity in m.s^{-1}, ρ is the air density in kg.m^{-3} and c is the speed of sound in m.s^{-1}. We implemented the FDTD method to solve those equations.

2.2. Spatial domain

The computational domain measures 10 m $\times$10 m $\times$10 m and discretized into a uniform Cartesian staggered grid of 25 mm resolution (i.e. 400 grid points in each direction). To lower the computational burden, a moving window feature was implemented that shifts the computational domain along the positive x-axis as the wavefront propagates. This dynamically moving window was described in [11].

The source $S(x_s, y_s, z_s)$ is placed at the center of the cubic computational domain at initial time. A receiver $R(x_r, y_r, z_r)$ is placed 100 m away from the source along the x-axis with $y_s = y_r$ and $z_s = z_r$, so the propagation is horizontal. The ground is assumed to be perfectly reflective and a perfectly matched layer (PML) is placed in the other five directions. For computational efficiency, the PML in the positive x-axis is removed since the wavefront never reaches this boundary of the moving window. Figure 1 summarizes the spatial 3D setup.

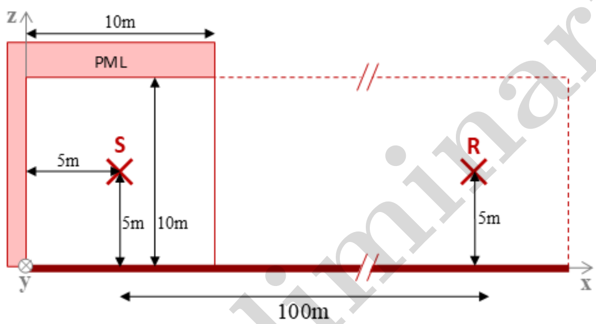

Figure 1: 2D illustration of the spatial 3D setup at initial time.

2.3. Temporal domain

The source S is defined as a soft Gaussian impulse point that evolves over time t as follows:

$$
p(x_s, y_s, z_s, t) = \exp\left(-\frac{1}{2} f_0^2 (t - t_0)^2\right) \tag{2}
$$

with p the acoustic pressure in Pa, f_0 the characteristic frequency set to 2 kHz and t_0 the offset time set to $\frac{10}{f_0} = 5\ \mu$s.

For this propagation geometry, it takes the direct wavefront 0.31 s to reach and surpass the receiver R, 100 m away from the source. As a consequence, 8 217 iterations are needed for a time step $dt = 37.8\ \mu$s, respecting the Courant–Friedrichs–Lewy condition [12].

2.4. Meteorological conditions

Four meteorological conditions are simulated and described in Table 1 by three atmospheric parameters: u_* is the friction velocity in m/s, Q_H is the surface sensible heat flux in W/m^2 and the boundary layer height z_i in m.

Condition	u_*	Q_H	z_i
(a)	0.1	50	1000
(b)	0.1	200	2000
(c)	0.5	50	1000
(d)	0.5	200	2000

Table 1: Atmospheric parameters of the four meteorological conditions simulated.

For all four meteorological conditions, the air temperature T_0 and the air density are constant in time and space, equal to 20°C and 1.2 kg/m^3 respectively.

3. Turbulence

The scattering of the acoustic wave by turbulence is numerically modeled with the help of the isotropic QW approach with no mean wind, described in [10] and based on [8], [9]. The notations from [10] are used in this work.

The QW are arranged by class size: the largest class size ($n = 1$) is defined according to the meteorological conditions of Table 1 and the next class is half the size of the previous one. For computational efficiency, the smallest class size ($n = N$) is limited to 0.343 m which caps the frequency analysis to 1 kHz. The total 3D field QW for the grid position (x, y, z) is the sum of the individual QW contributions QW^{mn} of each instance $m = 1, ..., N_n$ of every class size $n = 1, ..., N$:

$$
QW(x, y, z) = \sum_{n=1}^{N} \sum_{m=1}^{N_n} QW^{mn} \tag{3}
$$

This QW field is incorporated into a non-turbulent FDTD solver of outdoor sound propagation called *sonora* which is described in more detail in [11], [13]. We make the following assumptions when building the QW fields:

- the local variation of temperature and flow velocity are slower than the sound speed, so the turbulence is assumed to be frozen,
- the parent function of the QW is Gaussian: $f(x) = \exp(-\pi x^2/2)$,
- no fractional generations are introduced so the densification factor K is 1,
- the packing function of all class sizes is set to 10%,

3.1. Temperature-induced turbulence

For temperature induced turbulence, QW is a 3D scalar field and sums the temperature variation ΔT^{mn}

over n and m, defined at the grid position $r(x, y, z)$ as:

$$\Delta T^{mn}(x, y, z) = h^{mn} q_n \exp\left(-\frac{\pi}{2}\frac{|\mathbf{r} - \mathbf{b}^{mn}|^2}{a_n^2}\right) \quad (4)$$

with h^{mn} a random sign factor equal to $+1$ or -1 with equal probability, $\mathbf{b}^{mn}$ the random position inside the inner computational domain of the m^{th} instance of class size n, q_n the amplitude factor and a_n the length scale of size class n. The parameters q_n and a_n are calculated following the method explained in Chapter 11.2 of [10] so the calculations are not detailed here.
The temperature variations of temperature-induced turbulence are integrated via an effective speed of sound at the grid point $r(x, y, z)$:

$$c_{\text{eff}}(x, y, z) = \sqrt{\frac{\gamma R}{M}\left(T_0 + \sum_{n=1}^{N}\sum_{m=1}^{N_n} \Delta T^{mn}\right)} \quad (5)$$

with $\gamma = 7/5$ the adiabatic index, $R = 8.3145$ J.mol^{-1}.K^{-1} the molar gas constant and $M = 0.02896$ kg/mol the molar mass for dry air.
Figure 2 shows an example of the spatial field of the effective speed of sound using Eq. (5).

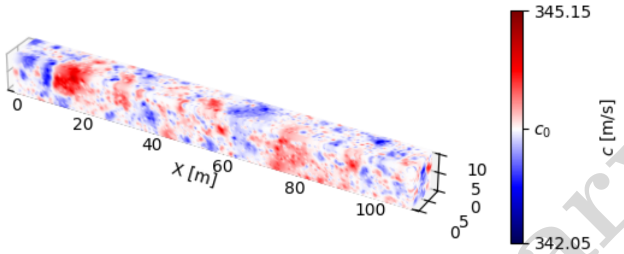

Figure 2: Effective speed of sound in the full computational inner domain for one simulation in the meteorological condition (d).

3.2. Velocity-induced turbulence

Similarly to the temperature-induced turbulence, the velocity-induced turbulence is modeled as the sum of the contribution of each QW; unlike the scalar QW field due to temperature-induced turbulence, the velocity-induced turbulence is a 3D vector field.
Following the sub-chapter 11.2.4 in [10], an individual velocity variation vector $\boldsymbol{\Delta}\mathbf{v}^{mn}$ at the grid point $r(x, y, z)$ is defined as:

$$\boldsymbol{\Delta}\mathbf{v}^{mn}(x, y, z) = a_n \pi \exp\left(-\frac{\pi}{2}\boldsymbol{\chi}^2\right)(\boldsymbol{\Omega}^{mn} \times \boldsymbol{\chi}) \quad (6)$$

with $\boldsymbol{\chi} = \frac{|\mathbf{r} - \mathbf{b}^{mn}|}{a_n}$ the magnitude vector and $\boldsymbol{\Omega}^{mn}$ the angular velocity vector. The magnitude of the $\boldsymbol{\Omega}^{mn}$ vector is again calculated following [10]. The orientation of $\boldsymbol{\Omega}^{mn}$ and the position $\mathbf{b}^{mn}$ are randomized.
Since we are interested in the wavefront moving in the positive x-direction, the cross-directional components of $\boldsymbol{\Delta}\mathbf{v}^{mn}$ (i.e. along the y- and z-axis) are neglected, and only the velocity variations of velocity-induced turbulence in the x-axis component are included in the effective speed of sound at the grid point (x, y, z):

$$c_{\text{eff}}(x, y, z) = \sqrt{\frac{\gamma R T_0}{M}} + \sum_{n=1}^{N}\sum_{m=1}^{N_n} \Delta v^{mn} \quad (7)$$

3.3. Metric

The accuracy of the QW model for representing atmospheric turbulence is evaluated using the coherence loss between the direct and ground-reflected waves due to turbulence at the receiver point R compared to a non-turbulent medium. For the non-turbulent atmosphere, the wave equation Equation (1) is solved for a constant speed of sound c. We get the acoustic pressure at the receiver p_{non} for the setup described in Section 2.2 and p_{ff} in the free field case, i.e. replacing the ground with a PML. The ground effect is the ratio in absolute value of the fast Fourier transform (noted as: $\tilde{}$) of p_{non} over p_{ff}:

$$\text{GE}_{\text{non}} = 10\log_{10}\frac{|\tilde{p}_{\text{non}}|^2}{|\tilde{p}_{\text{ff}}|^2}\ [\text{dB}] \quad (8)$$

For the four types of meteorological conditions, the field of effective speed of sound c_{eff} is calculated for every grid point in the inner computational domain. For the corresponding turbulent atmosphere, the wave equation Equation (1) is solved by replacing c with the c_{eff} to get the acoustic pressure at the receiver p_{turb}. The ground effect in a turbulent atmosphere is:

$$\text{GE}_{\text{turb}} = 10\log_{10}\frac{|\tilde{p}_{\text{turb}}|^2}{|\tilde{p}_{\text{ff}}|^2}\ [\text{dB}] \quad (9)$$

3.4. Theory

The numerical results are compared to the theoretical results provided by Ostashev in [10]. The mean square sound pressure for a perfectly reflective ground is:

$$\langle pp^* \rangle = \frac{1}{R_1^2} + \frac{1}{R_2^2} + \frac{2C_{\text{coh}}}{R_1 R_2}\cos\left(k(R_1 - R_2)\right) \quad (10)$$

with $R_1 = \sqrt{(x_s - x_r)^2 + (z_s - z_r)^2}$ the path length of the direct wave, $R_2 = \sqrt{(x_s - x_r)^2 + (z_s + z_r)^2}$ the path length of the ground-reflected wave, C_{coh} the coherence factor, and $k = 2\pi f/c_0$ the wave number. For a non-turbulent atmosphere, $C_{\text{coh}} = 1$.

The coherence factor for temperature-induced turbulence C_{coh}^T and velocity-induced turbulence C_{coh}^v for the von Kármán spectra is given in [14] by:

$$C_{\text{coh}}^T = \exp\Bigg(-\frac{2\gamma_T x_{sr} L_T}{h} \int_0^{\frac{h}{L_T}} 1 - \frac{2^{1/6}\eta^{5/6}}{\Gamma(5/6)} K_{5/6}(\eta) d\eta\Bigg) \quad (11)$$

$$C_{\mathrm{coh}}^{v} = \exp\Bigg(-\frac{2\gamma_v x_{sr} L_v}{h}$$

$$\int_0^{\frac{h}{L_T}} 1 - \frac{2^{1/6}\eta^{5/6}}{\Gamma(5/6)}\left(K_{5/6}(\eta) - \frac{\eta}{2}K_{1/6}(\eta)\right)d\eta\Bigg) \qquad (12)$$

with γ_T and γ_v the respective extinction coefficients for the von Kármán turbulence spectrum, $x_{sr} = 100$ m the distance between the source and the receiver, L_T and L_v the respective length scales of fluctuations, and h the maximum separation between direct and reflected path. The distance $h = 5$ m since the source and the receiver are both 5 m above the ground. $K_n(\eta)$ is the modified Bessel function of order n.
The theoretical ground effect is calculated as:

$$\mathrm{GE}_{\mathrm{coh}} = 10\log_{10}\langle pp^*\rangle - 10\log_{10}\frac{1}{R_1^2} \qquad (13)$$

with $\mathrm{TL}_{\mathrm{free}}$ the transmission loss at the receiver of a source radiating into a free space in a straight line, representing the direct path.

4. Results

The simulation results are generated by taking advantage of the parallel nature of the FDTD calculations and the computer hardware (NVIDIA RTX PRO 4500 Blackwell).

4.1. Non-turbulent atmosphere

The theoretical ground effect from Eq. (13) is compared to the numerical ground effect from Eq. (8) in a non-turbulent atmosphere, as shown in Figure 3.

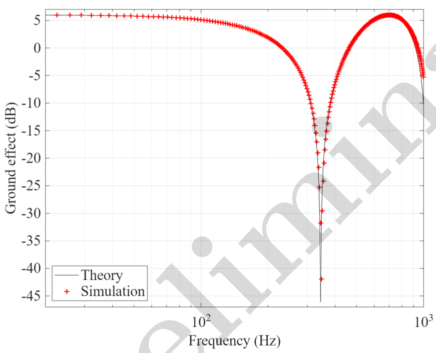

Figure 3: Spectral ground effect for a non-turbulent atmosphere.

In Figure 3, the numerical results GE_{non} closely match the theoretical ground effect GE_{coh} up to the upper limit of the selected frequency range.

4.2. Turbulent atmosphere

4.2.1. Temperature-induced turbulence

We ran 50 simulations for the four meteorological conditions of Table 1 with different randomized positions $\mathbf{b}^{mn}$ and signs h^{mn} that define the temperature variations of each QW in Eq. (4). Figure 4 shows the ground effect for 50 simulations, zoomed in a frequency window of 200 to 600 Hz.

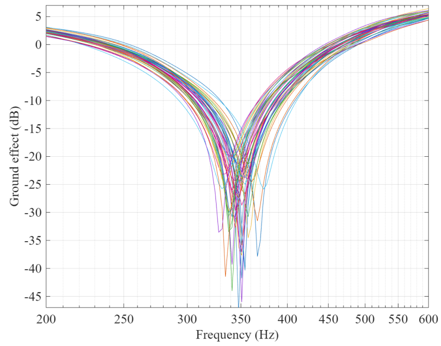

Figure 4: Spectral ground effect of 50 simulations ran with different turbulence realizations, for a temperature-induced turbulent atmosphere with meteorological condition (d).

The different configurations of QWs accelerates or decelerates the wavefront along the propagation paths. As a result, the interference of the direct and ground-reflected waves at receiver R is impacted. For example in the meteorological condition (d) as shown in Figure 4: at the first interference trough, the magnitude of the ground effect varies between -47.7 dB to -20.1 dB and the frequency varies over a 42 Hz range.
Table 2 shows the average total number of QW and the corresponding simulation time over the 50 simulation for the four turbulent cases for temperature-induced turbulence.

Condition	Number of QW	Simulation time (s)
(a)	34 244	256
(b)	35 408	258
(c)	116 204	377
(d)	154 977	435

Table 2: Average number of QW and corresponding simulation time for temperature-induced turbulence.

The energetic average over $|\tilde{p}_{\mathrm{turb}}|$ is then calculated to get the average ground effect GE_{turb} which is shown as a function of frequency in Figure 5 for the four meteorological conditions.
The four average ground effect GE_{turb} closely match their corresponding theoretical ground effect GE_{coh} linked to coherence loss using the factor Eq. (11). Despite the variability of the effect of QWs on the sound propagation (as shown in Figure 4), the turbulent field is designed so that over a sufficient number of simulations, the impact of atmospheric turbulence on the ground effect averages towards the expected theoretical ground effect.

4.2.2. Velocity-induced turbulence

Similarly, the QW field for velocity-induced turbulence produced by buoyancy is generated with random position $\mathbf{b}^{mn}$ and orientation for the vector $\mathbf{\Omega}^{mn}$.
In the case of buoyancy-produced turbulence, condition (a) and (b) are equivalent to (c) and (d), respectively, because this type of turbulence do not

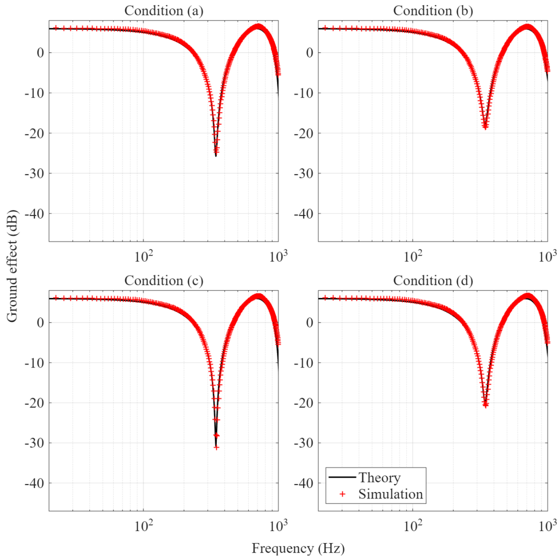

Figure 5: Averaged spectral ground effect for a temperature-induced turbulent atmosphere.

depend on u_*. We ran 50 simulations for conditions (a) and (b), and their average ground effect GE_{turb} is shown with the corresponding theoretical ground effect GE_{coh} in Figure 6. The average number is of QW is 93 600 and the average simulation time is 420s.

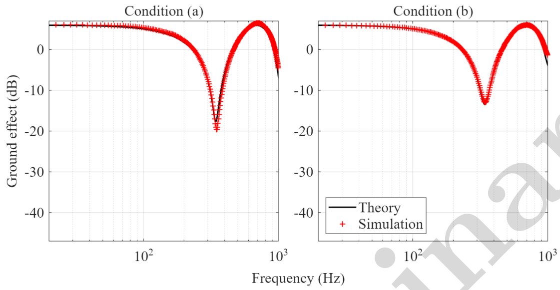

Figure 6: Averaged spectral ground effect for a buoyancy-produced turbulent atmosphere.

For a buoyancy-produced turbulence, the average ground effect GE_{turb} still matches their corresponding theoretical ground effect GE_{coh} linked to coherence loss using the factor Eq. (12).

In that case of shear-produced turbulence, condition (a) and (c) are equivalent to (b) and (d), respectively, because this type of turbulence do not depend on Q_H and z_i. We ran 50 simulations for conditions (a) and (c), and the results are shown in Figure 7. The average number is of QW is 47 675 and the average simulation time is 315 s.

For a velocity-induced turbulence produced by wind shear, the average ground effect shows a loss of coherence but not to the same extent than expected with the corresponding theoretical ground effect. At the first interference trough, GE_{turb} is around 7 dB lower than GE_{coh}. This gap may be explain by the anisotropy of the shear-layer model which was not

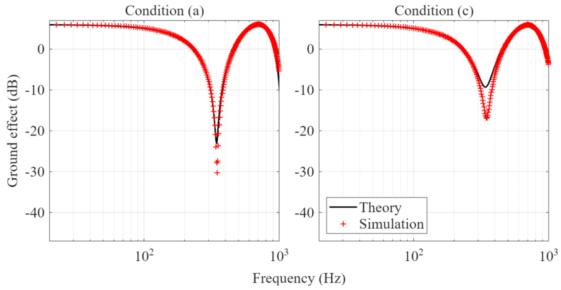

Figure 7: Averaged spectral ground effect for a shear-produced turbulent atmosphere.

taken into account for the isotropic QW model of turbulence in this work.

4.2.3. Combined effect

Finally, the combined effect of the three types of turbulence is evaluated. We ran 50 simulations for the four meteorological conditions of Table 1 and the results are shown in Figure 8.

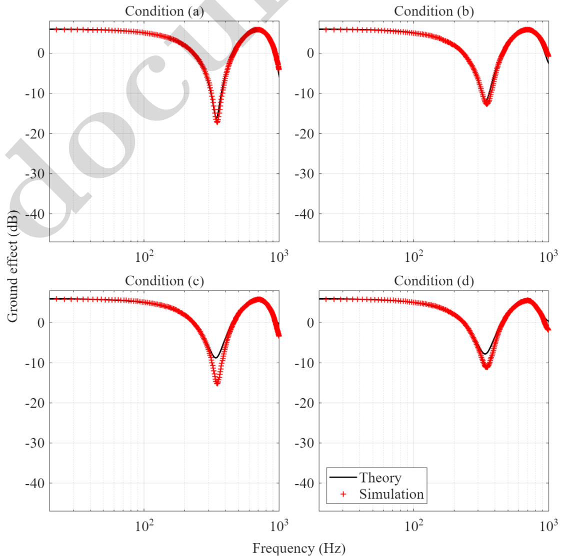

Figure 8: Averaged spectral ground effect for a combined turbulent atmosphere.

For the combined effect of the three types of turbulence, the theoretical ground effect GE_{coh} linked to coherence loss is calculated using the combined factor between Eq. (11) and Eq. (12). For the meteorological conditions (a) and (b), the friction velocity u_* is low (equal to 0.1 m/s) so the shear-produced turbulence is minor compared to the other types of turbulence. The simulation results of conditions (a) and (b) closely match the corresponding theoretical results, which is consistent with the conclusions from the isolated cases of temperature-induced and buoyancy-produced turbulence (see Fig. 5 and Fig. 6). For the meteorological conditions (c) and (d), u_* is high (equal to 0.5 m/s) so the effect of shear-produced turbulence is more pronounced than in the conditions (a) and (b). The GE_{turb} of conditions (c) and (d) both show a significant loss of coherence but not to the same extent than expected with the corresponding theoretical ground effect, which is consistent with the conclusion from the isolated case of shear-produced turbulence (see Fig. 7).

5. Conclusion

The isotropic quasi-wavelet approach is a practical way of including turbulence in the numerical modeling of outdoor sound propagation. This work extends the existing literature by partially validating the use of the FDTD method to model atmospheric turbulence with the quasi-wavelet approach. The atmospheric turbulence is modeled as a scalar quasi-wavelet field that introduces temperature and/or velocity variations at every grid point of the computational domain, affecting an effective speed of sound. For a long-range horizontal propagation near a perfectly reflective ground, the numerical results closely match the theoretical results in term of coherence loss between the direct and ground-reflected waves, except for velocity-induced turbulence produced by wind shear.

For a spatial computational domain of 11 000 m^3, the computation of each simulation lasts a reasonable amount of time, from 4 up to 7 min. The computational efficiency of *sonora* rely on the parallelization of the calculations when solving the 3D wave equation in the FDTD method, on the hardware used of the computation and on the moving window feature of the tool.

The results of this work suggests that the isotropic quasi-wavelet approach is a suitable strategy for the numerical modeling of some types of atmospheric turbulence with the FDTD method in outdoor sound propagation simulations. This approach will be applied in simulations of more complex situations, with for example non-flat terrains, obstacles, and more elaborate boundary conditions than perfectly reflective.

Acknowledgments

This research was supported by the international research project "Localization and Identification Of moving Noise sources" (LION 2). The Swiss contribution was funded by the Swiss National Science Foundation (Grant No. 223150).

References

[1] D. Botteldooren, "Acoustical finite difference time domain simulation in a quasi-cartesian grid.," *Journal of the Acoustic Society of America*, vol. 95, 1994.

[2] R. Blumrich and D. Heimann, "A linearized Eulerian sound propagation model for studies of complex meteorological effects," *Journal of the Acoustical Society of America*, vol. 112, 2002. DOI: 10.1121/1.1485971.

[3] V. E. Ostashev, D. K. Wilson, L. Liu, D. F. Aldridge, N. P. Symons, and D. Marlin, "Equations for finite-difference, time-domain simulation of sound propagation in moving inhomogeneous media and numerical implementation," *Journal of the Acoustical Society of America*, vol. 117, 2005. DOI: 10.1121/1.1841531.

[4] S. Cheinet, L. Ehrhardt, D. Juvé, and P. Blanc-Benon, "Unified modeling of turbulence effects on sound propagation," *Journal of the Acoustical Society of America*, vol. 132, 2012. DOI: 10.1121/1.4748584.

[5] C. Torrence and G. P. Compo, "A practical guide to wavelet analysis," *Bulletin of the American Meteorological Society*, vol. 79, 1998. DOI: 10.1175/1520-0477(1998)079<0061:APGTWA>2.0.CO;2.

[6] G. H. Goedecke and H. J. Auvermann, "Acoustic scattering by atmospheric turbules," *Journal of the Acoustical Society of America*, vol. 102, 1997. DOI: 10.1121/1.419951.

[7] G. H. Goedecke, V. E. Ostashev, D. K. Wilson, and H. J. Auvermann, "Quasi-Wavelet Model of Von Kármán Spectrum of Turbulent Velocity Fluctuations," *Boundary-Layer Meteorology*, vol. 112, 2004. DOI: 10.1023/B:BOUN.0000020158.10053.ab.

[8] G. H. Goedecke, D. K. Wilson, and V. E. Ostashev, "Quasi-Wavelet Models of Turbulent Temperature Fluctuations," *Boundary-Layer Meteorology*, vol. 120, 2006. DOI: 10.1007/s10546-005-9037-1.

[9] D. K. Wilson, V. E. Ostashev, and G. H. Goedecke, "Quasi-wavelet formulations of turbulence and other random fields with correlated properties," *Probabilistic Engineering Mechanics*, vol. 24, 2009. DOI: 10.1016/j.probengmech.2008.09.002.

[10] D. K. W. Vladimir E. Ostashev, *Acoustics in Moving Inhomogeneous Media*. CRC Press, 2026. DOI: 10.1201/9781003187912.

[11] H. Montanaro, D. Lincke, T. Van Renterghem, K. Heutschi, and R. Pieren, "Memory Efficient GPU-accelerated 3D FDTD Acoustic Simulations in Turbulent Fields," in *Forum Acusticum 2023: 10th Convention of the European Acoustics Association*, 2023.

[12] R. Courant, K. Friedrichs, and H. Lewy, "On the partial difference equations of mathematical physics," *IBM J. Res. Dev.*, vol. 11, no. 2, 1967. DOI: 10.1147/rd.112.0215.

[13] H. Montanaro, J. Knöpfel, K. Heutschi, and R. Pieren, "Parallelized FDTD Simulations to improve engineering models of urban road traffic noise," in *24th international congress on acoustics*, 2022.

[14] K. Attenborough and T. Van Renterghem, *Predicting Outdoor Sound*, 2nd ed. CRC Press, 2021. DOI: 10.1201/9780429470806.